Geophys. J. Int. (2008) **172,** 1016–1032 doi: 10.1111/j.1365-246X.2007.03685.x

Global anisotropic phase velocity maps for higher mode Love and Rayleigh waves

K. Visser,[1] J. Trampert[1] and B. L. N. Kennett[2]

[1] *Department of Earth Sciences, Utrecht University, Utrecht* 3584 CD*, The Netherlands. E-mail: kvis@geo.uu.nl*
[2] *Research School of Earth Sciences, The Australian National University, Canberra, Australia*

Accepted 2007 November 6. Received 2007 October 22; in original form 2007 May 4

SUMMARY

It is well established that the Earth's uppermost mantle is anisotropic, but there are no clear observations of anisotropy in the deeper parts of the mantle. Surface waves are well suited to observe anisotropy since they carry information about both radial and azimuthal anisotropy. Fundamental mode surface waves, for commonly used periods up to 200 s, are sensitive to structure in the first few hundred kilometres, and therefore, do not provide information on anisotropy below. Higher mode surface waves have sensitivities that extend to and beyond the transition zone, and should thus give insight about azimuthal anisotropy at greater depths. We have measured higher mode Love and Rayleigh phase velocities using a model space search approach, which provides us with consistent relative uncertainties from measurement to measurement and from mode to mode. From these phase velocity measurements, we constructed global anisotropic phase velocity maps. Prior to inversion, we determine the optimum relative weighting for anisotropy. We present global azimuthal phase velocity maps for higher mode Rayleigh waves (up to the sixth higher mode) and Love waves (up to the fifth higher mode) with corresponding average model uncertainties. The anisotropy we derive is robust within the uncertainties for all modes. Given the ray theoretical sensitivity kernels of Rayleigh and Love wave modes, the source of anisotropy is complex, but mainly located in the asthenosphere and deeper. Our models show a good correspondence with other studies for the fundamental mode, but we have been able to achieve higher resolution.

Key words: Inverse theory; Surface waves and free oscillations; Seismic anisotropy; Seismic tomography.

1 INTRODUCTION

It is widely established that the Earth's upper mantle is anisotropic. The first observation of radial anisotropy was the discrepancy between Rayleigh and Love wave dispersion observed by Anderson (1961), Aki & Kaminuma (1963) and McEvilly (1964). Anisotropy was also observed in the azimuthal dependence of P_n velocities (Hess 1964) and *S*-wave splitting in teleseismic *SKS* waves (Vinnik & Romanowicz 1989). The first observation of azimuthal anisotropy, the azimuthal variation of phase velocities, was noted by Forsyth (1975) in the Pacific Ocean. Radial and azimuthal anisotropy are both observed by surface waves, which is why these waves are well suited to study anisotropy. Radial and azimuthal anisotropy are the result of the same underlying anisotropy of the Earth's interior and were linked in a common mathematical framework by Montagner & Nataf (1986). The alignment (lattice preferred orientation or LPO) of intrinsically anisotropic minerals under strain in the mantle is assumed to be the major cause of upper-mantle anisotropy (Karato 1998; Montagner 1998). Anisotropy is thus an indicator of mantle deformation and flow. Therefore, it is critical to image anisotropy to understand the dynamics of the mantle.

Fundamental mode surface waves are well suited to provide information about anisotropy in the upper mantle (Nataf *et al.* 1984; Tanimoto & Anderson 1984; Montagner & Tanimoto 1991; Ekström & Dziewonski 1998). The sensitivity of fundamental mode surface waves for commonly used periods up to 200 s is however limited to the upper 400 km of the Earth's mantle. The use of higher mode surface waves should increase our knowledge of anisotropy into the lower part of the upper mantle and the upper part of the lower mantle due to their greater sensitivity at depth compared to fundamental mode surface waves. In the last few years higher mode surface waves have been added to studies of anisotropy (Debayle & Kennett 2000; Simons *et al.* 2002; Trampert & van Heijst 2002; Beucler & Montagner 2006; Maggi *et al.* 2006). The number of higher modes used in these studies varies due to the difficulty of measuring higher mode phase velocity, especially for Love waves since the higher modes arrive simultaneously with the fundamental mode. Trampert & van Heijst (2002) and Beucler & Montagner (2006) use phase velocities up to the second higher mode and Debayle & Kennett (2000) and Maggi *et al.* (2006) use phase velocities up to the fourth higher mode. The number of measurements are often few (Debayle & Kennett 2000) sometimes imposed by the clustering of events

(Beucler & Montagner 2006; Maggi *et al.* 2006; Sebai *et al.* 2006) and the geographical coverage is limited.

This study presents global azimuthal anisotropic phase velocity maps for fundamental and higher mode Love and Rayleigh waves up to the sixth higher mode consisting of a large number of measurements with consistent standard deviations. The phase velocities were measured using a model space search approach (Yoshizawa & Kennett 2002; Visser *et al.* 2007) which provides realistic consistent uncertainties on the phase velocity measurements. Following Trampert & Woodhouse (2003), we determine the optimum relative weighting of anisotropy prior to inversion and present global azimuthal anisotropic phase velocity maps up to the fifth higher mode for Love and up to the sixth higher mode for Rayleigh.

Finally, we analyse the resolution of the azimuthal anisotropic phase velocity maps and look at spectral leakage and trade-offs in particular. Spectral leakage is the effect of mapping small-scale structure not accounted for in the model expansion into the inverted low-degree structure. It arises as a result of uneven data coverage (Snieder *et al.* 1991). We suppress spectral leakage by using Laplacian damping, which increases the damping with increasing degree. This process effectively decreases the spectral leakage (Spetzler & Trampert 2003) but also decreases resolution for higher and higher degrees. By looking at the off-diagonal terms of the resolution matrix, we find that the trade-off between parameters remains acceptably small.

2 PHASE VELOCITY MEASUREMENTS

We follow the approach of Yoshizawa & Kennett (2002) and measure phase velocities using a model space approach (Visser *et al.* 2007). In principle, the model space search to invert for a 1-D velocity model could include the full non-linearity of the forward problem. This is very time consuming, and therefore, we chose to linearize the forward problem by centring the model space search around a reference model and using the Fréchet derivatives of this reference model to calculate the synthetic seismograms. This inherently introduces a dependence on the chosen reference model and the requirement that the chosen reference model should be close to our final model. We use the automated multimode inversion (AMI, Lebedev *et al.* 2005) to obtain a reference model for the model space search. AMI is a non-linear waveform inversion in multiple time and frequency windows which obtains the best shear wave velocity model that fits the seismogram. The time and frequency windows are chosen such that both the fundamental mode and the higher modes are fitted. AMI also applies strict data quality criteria and ensures the validity of the JWKB approximation. The shear velocity model from AMI is close to the best shear wave velocity model which we find in the model space search. Differences between both models are small and largely due to the use of different parametrizations for the shear wave velocity models. AMI uses around 18 boxcar and triangle functions up to 1500 km and we use 12 natural cubic spline functions that span the crust, upper mantle and lower mantle up to a depth of 1500 km. We have experimented with the number and position of the spline functions and found that this parametrization is sufficient to resolve up to the fifteenth higher mode. We do not expect to resolve more than six higher modes which makes this parametrization more than sufficient for our purpose. The parametrization is more dense in the crust and upper mantle to match the expected depth resolution of surface waves. The difference between AMI and the model space search is that the first gives us one best fitting shear wave velocity model and the second gives us the whole ensemble of shear wave velocity models compatible with the seismograms which enables us to determine uncertainties. If we were only interested in the best fitting model, AMI would be sufficient. It is important to understand that AMI solves an ill-posed non-linear inverse problem. A solution is found by careful regularization, but other solutions exist compatible within the data errors. A Monte Carlo search around the AMI solution finds all those other models and allows us to determine meaningful uncertainties for the best fitting model. Usually, a model space search is used to solve highly non-linear problems. We use it to map the nullspace of a linearized problem instead.

Table 1. Frequency–time windows.

	Windows (t, ω)	
f (mHz)	Rayleigh (km s^{-1})	Love (km s^{-1})
5–10	3.7 ± 0.75	b - 3.8
10–20	3.75 ± 0.55	b - 3.8
	b - 4.3	
20–50	b - 4.3	b - 4.3

Note: Definition of frequency–time windows for Rayleigh and Love seismograms. The time windows are defined using the group velocity (km s^{-1}).

For the model space search we use the Neighbourhood Algorithm (NA, Sambridge 1999a). We search for the best fitting shear wave velocity model using a least-squares misfit between the data and the synthetic seismogram defined in multiple time and frequency windows, see Table 1. The frequency and time windows are chosen such that the fundamental and higher modes are included in the windows. For Love waves, it is not possible to separate the fundamental and higher modes since the group velocities are similar, thus we use a single time window for both waveforms. For Rayleigh waves, we separated the fundamental and higher mode waveforms in different time windows. The time b in Table 1 depends on the epicentral distance, below 35° the time is set just before the arrival of the *S* wave train, between 35° and 70° the time is set just after the *S* and before the *SS* wave train, etc. The synthetic seismograms are calculated using the JWKB approximation and the Fréchet derivatives which relate the change in compressional wave velocity, shear wave velocity and density from the reference model to a change in phase velocity. The compressional wave perturbations and the density perturbations are of secondary importance, thus we decided to scale these perturbations to the shear wave velocity perturbations thereby reducing the amount of parameters needed for the model space search. This choice significantly speeds up the model space search. For Rayleigh waves, we scale the compressional wave perturbations to the shear wave velocity perturbations with the scaling relation ($\mathcal{R} = \partial V_s/\partial V_p$) from Ritsema & Van Heijst (2002). $\mathcal{R}$ increases linearly from 1.25 at the surface to 3.0 at the CMB. For Love and Rayleigh waves, the density perturbations are scaled to the shear wave perturbations using ($\xi = \partial ln\rho/\partial lnV_s$) from Deschamps *et al.* (2001). ξ varies between -0.1 and 0.2. The attenuation model employed is that of PREM (Dziewonski & Anderson 1981).

The model space search provides us with an ensemble of shear wave velocity models and their fit to the data. This ensemble is resampled and transformed into a probability density surface in the second part of the NA (Sambridge 1999b). The resampling algorithm can also be used to evaluate Bayesian indicators of any transformed parameters that are a combination of the original parameters, in an identical manner to the original variables. We introduce phase velocity parameters defined for certain modes and periods since phase velocities may be obtained by integrating a shear wave velocity model using the sensitivity kernels for the specific mode and

period. The sensitivity kernels are calculated for the reference model, which is the best shear wave velocity model that we obtained from AMI. We thus obtain a probability density surface for our original (shear wave velocity) parameters and transformed (phase velocity) parameters. From the probability density surface we can obtain 1-D marginals for each original/transformed parameter by integrating over all other original/transformed parameters. The advantage of our approach is that now we are able to solve for phase velocities for multiple modes and periods without having to separate the modes and without too much computation time. The shape of the phase velocity marginals is Gaussian, and therefore, we represent the 1-D marginals as a mean phase velocity and a standard deviation. The phase velocities are presented as changes with respect to PREM for convenience.

In the resampling process, we introduced specific phase velocity parameters which are obtained by integrating each resampled shear wave velocity model using the corresponding sensitivity kernel. In theory, we could obtain phase velocities for every higher mode and period. In practise, we know that not all higher modes are constrained by the seismogram. To evaluate the number of modes constrained in each seismogram we calculated the unexplained variance which is defined as the least-squares misfit between the data and the synthetic normalized by the data. The unexplained variance is calculated as a function of the number of modes used in the synthetic seismogram calculation. For a perfect match between data and synthetic, the unexplained variance is zero. Since we calculate the unexplained variance only in the higher mode windows (Table 1: two windows for Rayleigh, the middle and highest frequency band; and one window for Love, the highest frequency band), the unexplained variance is unity for a fundamental mode synthetic seismogram and should decrease to zero for a perfect full synthetic seismogram. The unexplained variance, therefore, is a function which, in practise, has its maximum for the fundamental mode only and decreases to some constant value for increasing higher modes. This determines the number of modes needed to explain the specific seismogram. The number of higher modes we measure is defined as the smallest number of higher modes which brings the unexplained variance below 25 per cent of its range, where the range is defined as the difference between the largest and the smallest unexplained variance. Further details may be found in Visser *et al.* (2007).

The unexplained variance is also used to check when we obtain an overall bad fit for the higher modes and whether the seismogram contains no significant higher mode information. In such cases we decide to only measure the fundamental mode. Finally, if we obtain a bad fit for the whole seismogram (unexplained variance larger than 0.4), we discard the measurements.

We measured phase velocities for fundamental and higher mode Love and Rayleigh waves for seismograms that were recorded at the stations of the GDSN and GEOSCOPE networks from 1994 to 2004. The azimuthal coverage for the higher mode Rayleigh and Love wave measurements are shown in Figs 1 and 2. We do not show the azimuthal coverage for the fundamental mode since it is similar to the minor arc coverage given by Trampert & Woodhouse (2003) for Rayleigh and Love waves. The number of measurements

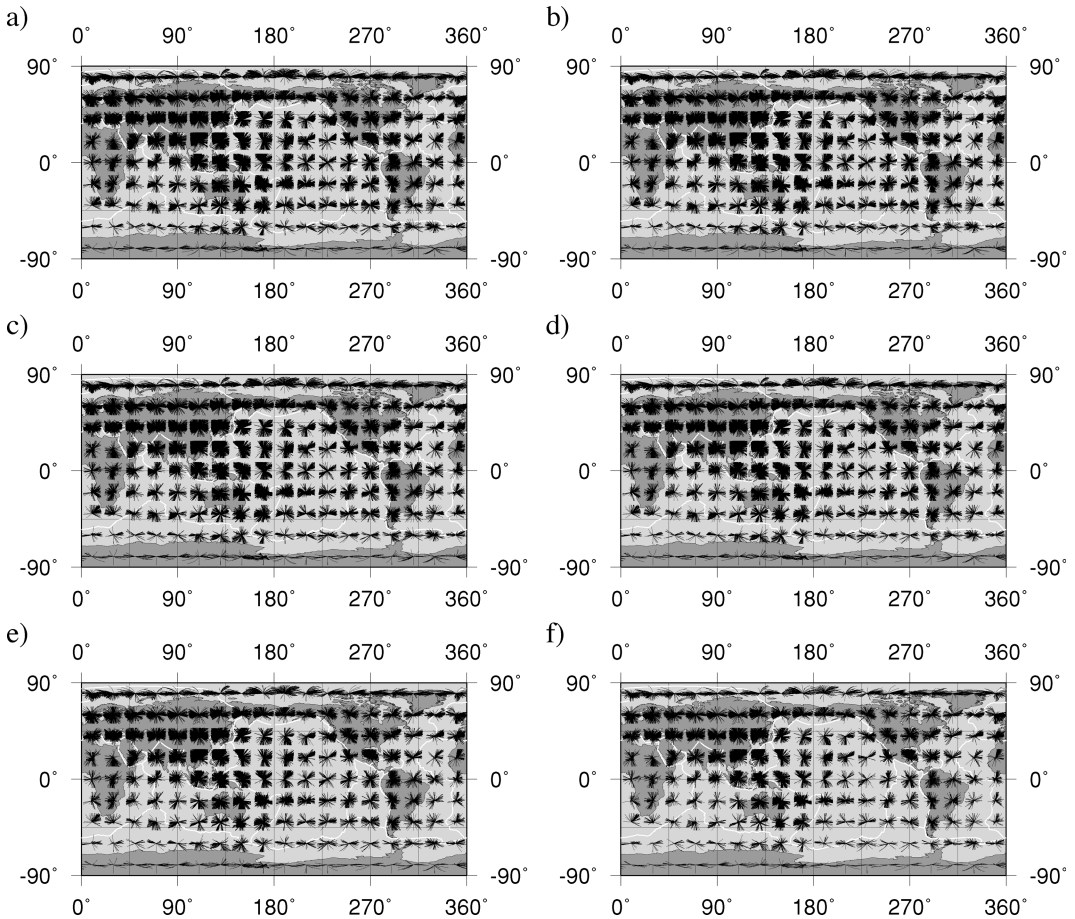

Figure 1. Minor arc Rayleigh wave azimuthal coverage for first higher mode (a), second higher mode (b), third higher mode (c), fourth higher mode (d), fifth higher mode (e) and sixth higher mode (f).

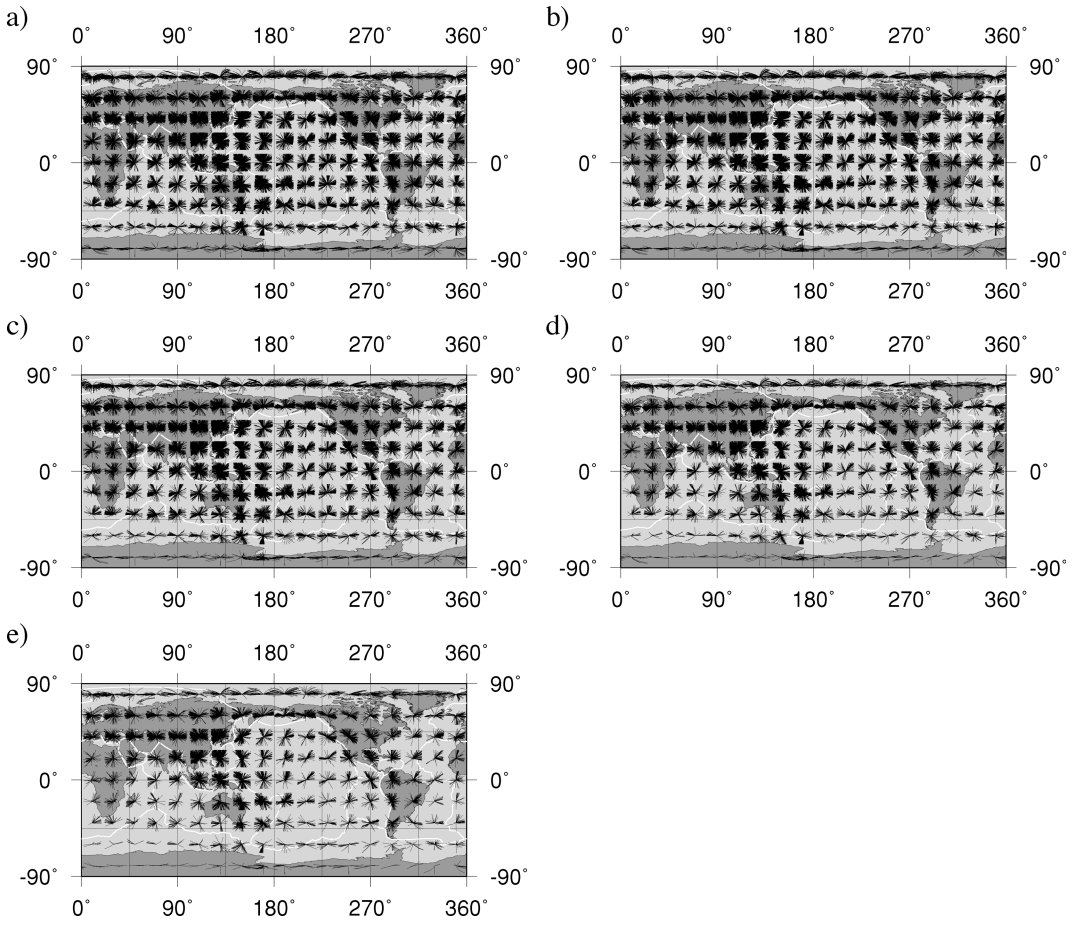

Figure 2. Minor arc Love wave azimuthal coverage for first higher mode (a), second higher mode (b), third higher mode (c), fourth higher mode (d) and fifth higher mode (e).

Table 2. Number of measurements.

	Number of measurements	
	Rayleigh	Love
Fundamental mode	63 628	45 179
First higher mode	54 035	34 859
Second higher mode	52 457	31 704
Third higher mode	48 762	24 102
Fourth higher mode	40 606	15 065
Fifth higher mode	31 637	8514
Sixth higher mode	21 626	

Note: Number of minor arc phase velocity measurements for Rayleigh and Love wave fundamental and higher modes.

obtained for the fundamental and each of the higher modes is shown in Table 2. We obtain the highest number of measurements for the fundamental mode followed by the first, second, third, etc., higher modes. As explained above, the unexplained variance will decrease as the number of higher modes increases. For a seismogram with less higher mode information the unexplained variance decreases more rapidly and the number of higher modes we decide to measure is less. Also, noisier seismograms will lead to less higher modes that will be measured due to the faster decrease of the unexplained variance to an almost constant value. The almost constant value for higher modes indicates that we are trying to measure overtones not constrained by the seismogram which is why we have to restrict the number of higher modes we measure. Finally, the number of seismograms with significant second higher mode information will be less than the number of seismograms with significant first higher mode information and so on. This is mainly due to the smaller amplitudes of the higher modes which makes the contribution to the unexplained variance smaller. We also obtain more measurements for Rayleigh than for Love waves, because of the higher noise levels for Love wave seismograms.

3 AZIMUTHAL ANISOTROPY

In a slightly anisotropic medium the azimuthal dependence of the local phase velocities of Rayleigh and Love surface waves is described as (Smith & Dahlen 1973, 1975; Romanowicz & Snieder 1988; Larsen *et al.* 1998).

$$\frac{\mathrm{d}c}{c_0}(\omega, \psi) = \alpha_0(\omega) + \alpha_1(\omega)\cos(2\psi) + \alpha_2(\omega)\sin(2\psi) + \alpha_3(\omega)\cos(4\psi) + \alpha_4(\omega)\sin(4\psi), \quad (1)$$

where dc/c_0 is the relative phase velocity perturbation with respect to a spherically symmetric earth model, ω the radial frequency and ψ is the azimuth along the path. We follow the approach of Trampert & Woodhouse (2003) where the local phase velocity perturbation is expanded in terms of generalized spherical harmonics. This reduces eq. (1) to

$$\mathbf{d} = \mathbf{Gm}. \quad (2)$$

Table 3. Difference in χ^2 at the 99 per cent significance level determined by the F-test.

	$N-M$							
χ^2	7500	10 000	15 000	20 000	30 000	40 000	50 000	65 000
1.0	0.029	0.025	0.021	0.018	0.015	0.013	0.011	0.010
1.5	0.044	0.038	0.032	0.027	0.022	0.019	0.017	0.015
2.0	0.059	0.051	0.042	0.036	0.029	0.025	0.023	0.020
2.5	0.073	0.063	0.053	0.045	0.037	0.032	0.029	0.025
3.0	0.088	0.076	0.063	0.054	0.044	0.038	0.034	0.030
3.5	0.103	0.089	0.074	0.063	0.051	0.044	0.040	0.035
4.0	0.117	0.101	0.084	0.072	0.059	0.051	0.048	0.040

Note: The difference in χ^2 as a function of the χ^2 and the number of independent parameters ($N-M$).

Here $\mathbf{d}$ are the path-averaged phase velocity measurements, $\mathbf{m} = (\mathbf{m}_0, \mathbf{m}_2, \mathbf{m}_4)^T$ is the model vector corresponding to the spherical harmonic coefficients of the 0ψ, 2ψ and 4ψ terms. $\mathbf{G} = \text{diag}\,(\mathbf{G}_0, \mathbf{G}_2, \mathbf{G}_4)$ is the block diagonal matrix of the path-averaged spherical harmonics, for the 0ψ, 2ψ and 4ψ terms. The number of unknowns is $(L+1)^2$ for the 0ψ terms, $(2L+6)(L-1)$ for the 2ψ terms and $(2L+10)(L-3)$ for the 4ψ terms. We choose $L = 40$ for the isotropic term (0ψ) and $L = 20$ for the azimuthal terms (2ψ,4ψ), resulting in 3405 unknowns.

The inverse problem is solved by minimizing the cost function

$$C = (\mathbf{d}-\mathbf{Gm})^T\mathbf{C}_d^{-1}(\mathbf{d}-\mathbf{Gm}) + \mathbf{m}^T\mathbf{C}_m^{-1}\mathbf{m}, \tag{3}$$

where $\mathbf{C}_d$ is the diagonal data covariance matrix which consists of the squared standard deviations of the phase velocity measurements which are obtained from the model space search. $\mathbf{C}_m$ is the diagonal model covariance, used to impose Laplacian smoothing. In its partitioned form the expressions are

$$(C_{m_o})_{jj} = \frac{1}{\lambda}\frac{1}{[l(l+1)]^2} \tag{4}$$

$$(C_{m_2})_{jj} = \frac{\theta_2}{\lambda}\frac{1}{[l(l+1)]^2} \tag{5}$$

$$(C_{m_4})_{jj} = \frac{\theta_4}{\lambda}\frac{1}{[l(l+1)]^2}, \tag{6}$$

where λ is an overall damping parameter which controls the trade-off between the data misfit and smoothness. The parameters θ_2 and θ_4 control the relative strength of the anisotropy. For example, a value of 0.1 would give 10 times more weight to the isotropic terms relative to the anisotropic terms. Different values for θ_2 and θ_4 can be used to determine whether the data has a preference for anisotropy and if so, a preference for the 2ψ terms or for the 4ψ terms or for both.

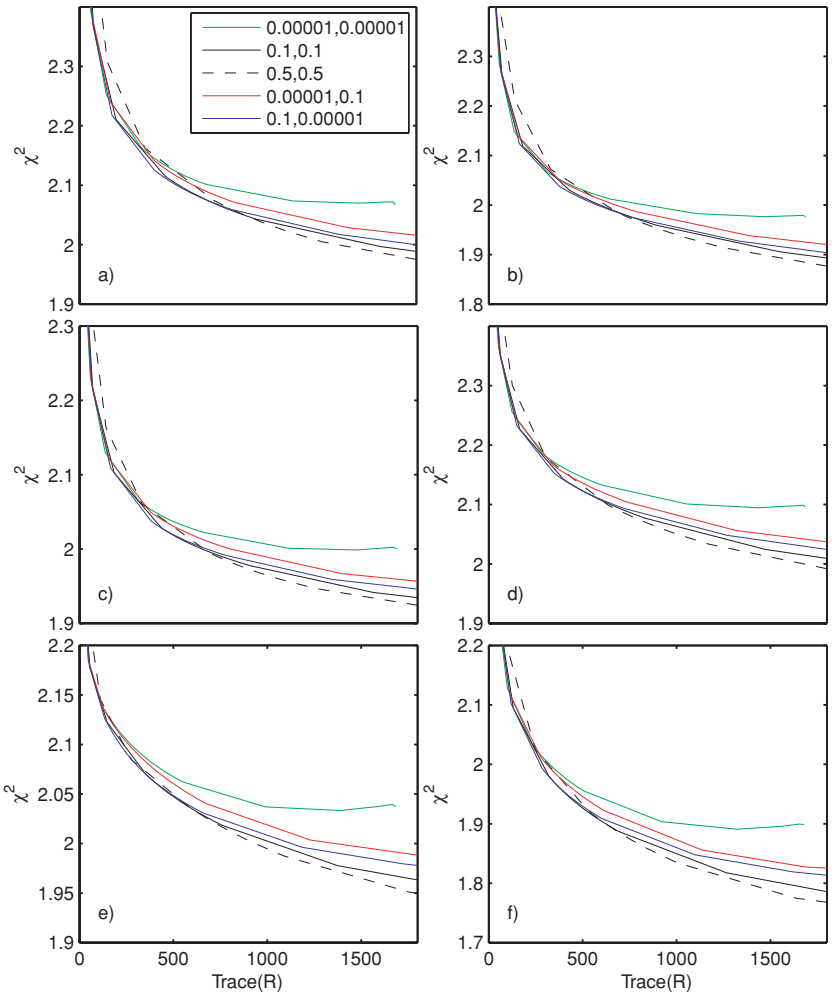

Figure 3. Misfit curves for Rayleigh (a) first higher mode at 148.56 s, (b) second higher mode at 40.028 s, (c) third higher mode at 77.795 s, (d) fourth higher mode at 35.078 s, (e) fifth higher mode at 56.074 s and (f) sixth higher mode at 35.141 s. The legend shows different values for θ_2 and θ_4.

To compare inversions with different regularizations, we define, a reduced χ^2 as

$$\chi^2 = \frac{1}{N-M}(\mathbf{d}-\mathbf{Gm})^T\mathbf{C}_d^{-1}(\mathbf{d}-\mathbf{Gm}), \quad (7)$$

where N is the number of data and M the trace of the resolution matrix. As the overall damping λ decreases, the trace of the resolution matrix (number of independent parameters) will increase and the reduced χ^2 will decrease, even if the misfit does not. A standard F-test (Bevington & Robinson 1992) determines if the difference between two χ^2 values is significant. Table 3 shows for a given χ^2 and number of free parameters ($N-M$) the associated significant difference in χ^2 at the 99 per cent confidence level. The meaning is that if for a given $N-M$, two χ^2 differ by more than this value, we are 99 per cent sure that the misfit is better and that this inversion should be preferred.

4 MISFIT CURVES FOR THE HIGHER MODES

Following Trampert & Woodhouse (2003), we calculated misfit curves systematically changing λ for a fixed θ_2 and θ_4 for each of the higher modes to determine if the higher modes require anisotropy and if we can distinguish between the different anisotropic terms. The misfit curves (Figs 3 and 4) show that for a small number of independent parameters, the isotropic parametrization (θ_2, $\theta_4 = 10^{-5}$) explains the data best. As the number of independent parameters increases, the anisotropic parametrizations ($\theta_2, \theta_4 > 10^{-5}$) start to explain the data better than the isotropic parametrization. At around 500 independent parameters, the isotropic misfit curves flatten out, indicating that anisotropy is indeed required by the data, because they give a better misfit with a high confidence level. The F-test (Bevington & Robinson 1992) gives the level of confidence with which the differences between the misfit curves is significant. For example, the first higher mode Rayleigh has a total of about 50 000 free parameters (the number of measurements - the trace of the resolution matrix) and a χ^2 of around 2.0 (Fig. 3a). According to Table 3 the 99 per cent significant difference is 0.023. At a trace of 1000, the difference between the isotropic and anisotropic misfit curves is 0.024, indicating indeed that we need anisotropy to explain our results. Beyond a trace of about 500, the differences between the isotropic and anisotropic misfit curves for all Rayleigh wave modes (Fig. 3) are significant with a high confidence level, indicating that anisotropy is needed to explain the phase velocity measurements. There are differences in misfit curves for different levels of anisotropic scaling, but these differences are not significant with a high confidence level.

As for Rayleigh waves, the difference between the isotropic and anisotropic misfit curves is 99 per cent significant for all Love wave modes (Fig. 4). Again the data cannot distinguish between different levels of anisotropic scaling. For fundamental mode Love waves, we would expect a preference for the 4ψ term of anisotropy since

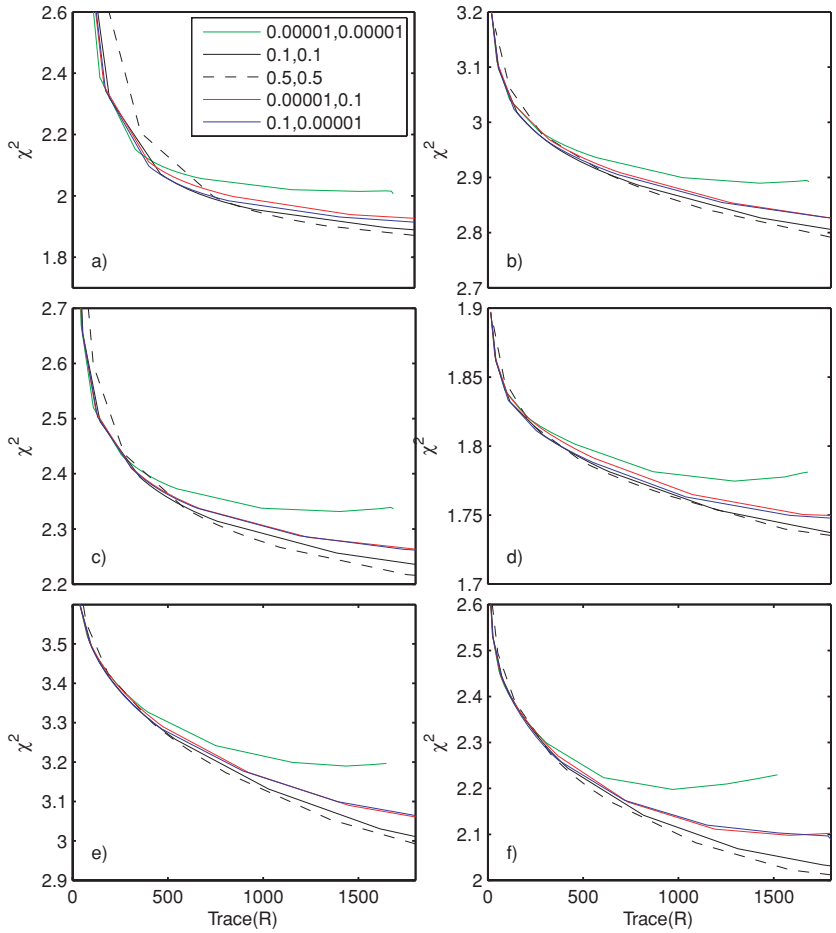

Figure 4. Misfit curves for Love (a) fundamental mode at 153.46 s, (b) first higher mode at 153.07 s, (c) second higher mode at 40.02 s, (d) third higher mode at 78.66 s, (e) fourth higher mode at 35.06 s and (f) fifth higher mode at 35.12 s.The legend shows different values for θ_2 and θ_4.

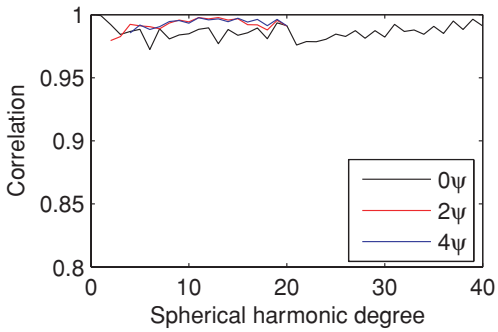

Figure 5. Correlation as a function of spherical harmonic degree for minor and major arc versus minor arc coverage.

the amplitude of the 4ψ sensitivity is much higher than the one for 2ψ. For higher mode Love waves, we do not expect a preference of one anisotropic term over the other since higher mode Love waves are sensitive to both the 2ψ as well as the 4ψ term of anisotropy. Earlier, a strong 2ψ term of anisotropy for fundamental Love waves has been found by Montagner & Tanimoto (1990). They ascribed this strong 2ψ term to Rayleigh–Love coupling, since fundamental mode sensitivity curves for Love waves only predict a strong 4ψ term of anisotropy. Trampert & Woodhouse (2003) found no statistical reason to include a 2ψ term and omitted it, based on asymptotic expectations. Since then, Sieminski *et al.* (2007) showed that Rayleigh–Love coupling is important (as speculated by Montagner & Tanimoto 1990) and results in a high near source sensitivity for azimuthal parameters B–H. Furthermore, tilted upper-mantle minerals with respect to the geographical reference system can result in high apparent values of B–H (Sieminski, personal communication, 2007). Although we find, similar to Trampert & Woodhouse (2003), no significant indication in favour of a 2ψ term, we choose to keep it based on a plausible reason for its existence. An important issue is to check whether the use of minor arc data alone (which results in poorer azimuthal coverage in the southern hemisphere) could bias our misfit curves. We computed synthetic data for a random anisotropic model (containing an isotropic, 2ψ and 4ψ term) and tested how well the random model could be retrieved by using a minor arc ray coverage alone and a minor and major arc ray coverage. We used the minor and major arc paths of Trampert & Woodhouse (2003). For the minor arc ray coverage we only took their minor arc paths. Fig. 5 shows the correlation between the model retrieved by the minor and major arc coverage and the model retrieved by the minor arc coverage only. The correlations are very high (>0.95), indicating that essentially the same model is retrieved using both the minor and major arc coverage and using the minor arc coverage only. We further established the important point that including the 2ψ term does not change the 4ψ models. In summary, beyond 500 independent model parameters, azimuthal anisotropy is required by the data for all modes of Love and Rayleigh waves considered here. The prior strength of anisotropy cannot be determined from the data and has to be fixed by other arguments.

5 AZIMUTHALLY ANISOTROPIC PHASE VELOCITY MAPS

We constructed azimuthally anisotropic phase velocity maps up to the first five higher mode Love and the first six higher mode Rayleigh

Table 4. The rms data uncertainty and resolution.

Mode	Period	σ_{dc/c_0}(per cent)	σ_{dc}(m s^{-1})	trace(**R**)	0ψ	2ψ	4ψ
			Rayleigh				
000s097	100.393	0.48	19.56	1008	695	146	167
000s197	51.259	0.60	23.54	965	665	140	160
001s068	99.650	0.53	31.16	947	651	139	156
001s156	50.855	0.56	28.24	938	644	138	156
002s056	99.258	0.48	34.00	961	660	141	160
002s137	50.849	0.56	32.16	930	639	137	154
003s120	51.059	0.56	36.46	918	631	135	152
003s201	35.014	0.57	32.35	929	638	137	154
004s109	51.052	0.56	40.06	889	610	132	147
004s183	35.078	0.59	36.51	880	604	130	146
005s101	50.921	0.58	44.59	841	576	126	139
005s168	35.115	0.60	40.87	832	571	124	137
006s096	50.822	0.61	49.99	768	526	116	126
006s157	35.141	0.59	42.49	772	528	117	127
			Love				
000t085	100.81	0.50	23.31	956	644	148	164
000t174	51.01	0.70	31.47	895	604	139	152
001t068	100.08	0.55	32.05	858	586	130	142
001t154	51.19	0.61	31.00	839	573	127	139
002t054	99.92	0.65	47.66	809	532	123	134
002t136	51.41	0.58	32.85	831	567	126	138
003t120	51.32	0.65	41.83	751	514	114	123
003t200	35.05	0.59	33.58	766	524	116	126
004t107	51.06	0.69	50.65	646	443	99	104
004t184	35.06	0.63	39.13	659	453	100	106
005t098	51.27	0.77	61.04	536	370	82	84
005t168	35.12	0.66	44.70	555	383	85	87

Note: Relative and absolute rms data uncertainties (σ_{dc/c_0} and σ_{dc}), the total number of independent parameters [trace(**R**)] and the number of independent parameters for the isotropic (0ψ), 2ψ and 4ψ models.

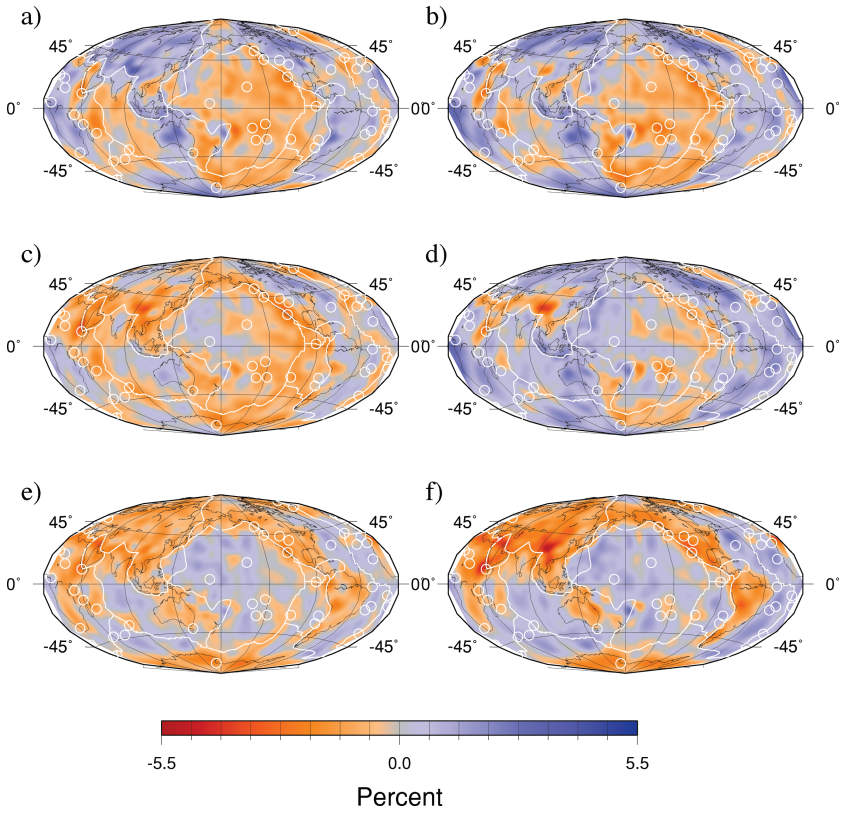

Figure 6. Relative isotropic phase velocity maps with respect to PREM for Rayleigh (a) first higher mode at 148.56 s, (b) second higher mode at 40.028 s, (c) third higher mode at 77.795 s, (d) fourth higher mode at 35.078 s, (e) fifth higher mode at 56.074 s and (f) sixth higher mode at 35.141 s.

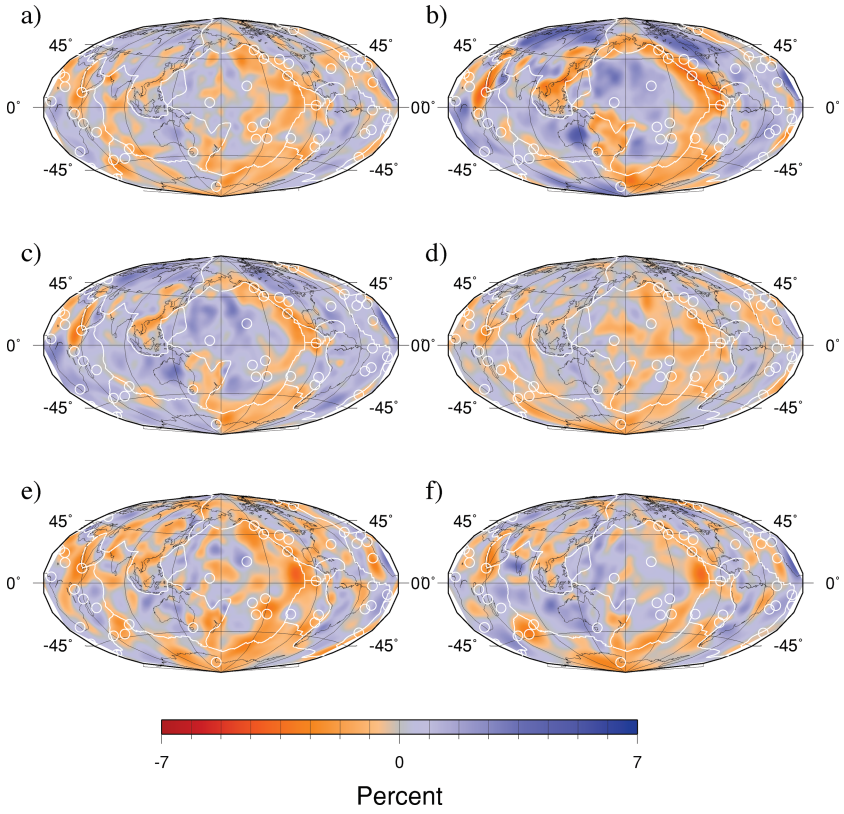

Figure 7. Relative isotropic phase velocity maps with respect to PREM for Love (a) first higher mode at 153.07 s, (b) first higher mode at 40.16 s, (c) second higher mode at 40.02 s, (d) third higher mode at 78.66 s, (e) fourth higher mode at 35.06 s and (f) fifth higher mode at 35.12 s.

wave phase velocities. The exact number of measurements used for the phase velocity maps is shown in Table 2 and the rms uncertainty of a sample of the data is shown in Table 4.

As seen in the previous paragraph, the data require azimuthal anisotropy but cannot decide upon its exact scaling. There is also no compelling reason to favour 2ψ or 4ψ terms only. An Occam-type argument guided us to choose a modest amount of anisotropy using $\theta_2 = \theta_4 = 0.1$. It should be noted that this is a prior constraint which will be overruled if the data require this locally. Because for fundamental modes our data quality seems superior compared to that used in Trampert & Woodhouse (2003), (smaller χ^2 for similar uncertainties in both data sets), we chose less overall damping to allow approximately 1000 independent parameters in the Rayleigh fundamental mode models. We have chosen an overall damping such that the relative model uncertainty remains constant for all modes. As a result, the phase velocity maps will have a decreasing resolution with increasing data uncertainty and/or decreasing number of data (see Table 4). This choice is somewhat arbitrary. In view of a future depth inversion, ideally, we should have chosen for a constant resolution. The difference in the number of data between modes, however, is so large that the corresponding decrease in overall damping would have led to unrealistic amplitudes in some higher mode maps. The other extreme would have been to opt for an increasing uncertainty because the number of data constraints decreases. This would lead to seriously overdamped higher mode maps. A constant relative uncertainty in the phase velocity maps is an acceptable compromise between the two extremes. The isotropic phase velocity maps were expanded up to degree and order 40, while the azimuthal anisotropic phase velocity maps were expanded up to degree and order 20.

The isotropic models for Rayleigh and Love waves are shown in Figs 6 and 7 for a number of different higher modes at the indicated periods. The fundamental mode maps are very similar to those of Trampert & Woodhouse (2003) with correlations of 0.91 (Rayleigh 40 s), 0.70 (Rayleigh 150 s), 0.87 (Love 40 s) and 0.79 (Love 150 s), and hence to other models by different research groups (see Becker *et al.* 2007, for a recent comparison). While the overtones generally show the strongest sensitivity to deeper mantle structure, it is interesting to note that high frequency Rayleigh waves of the fifth

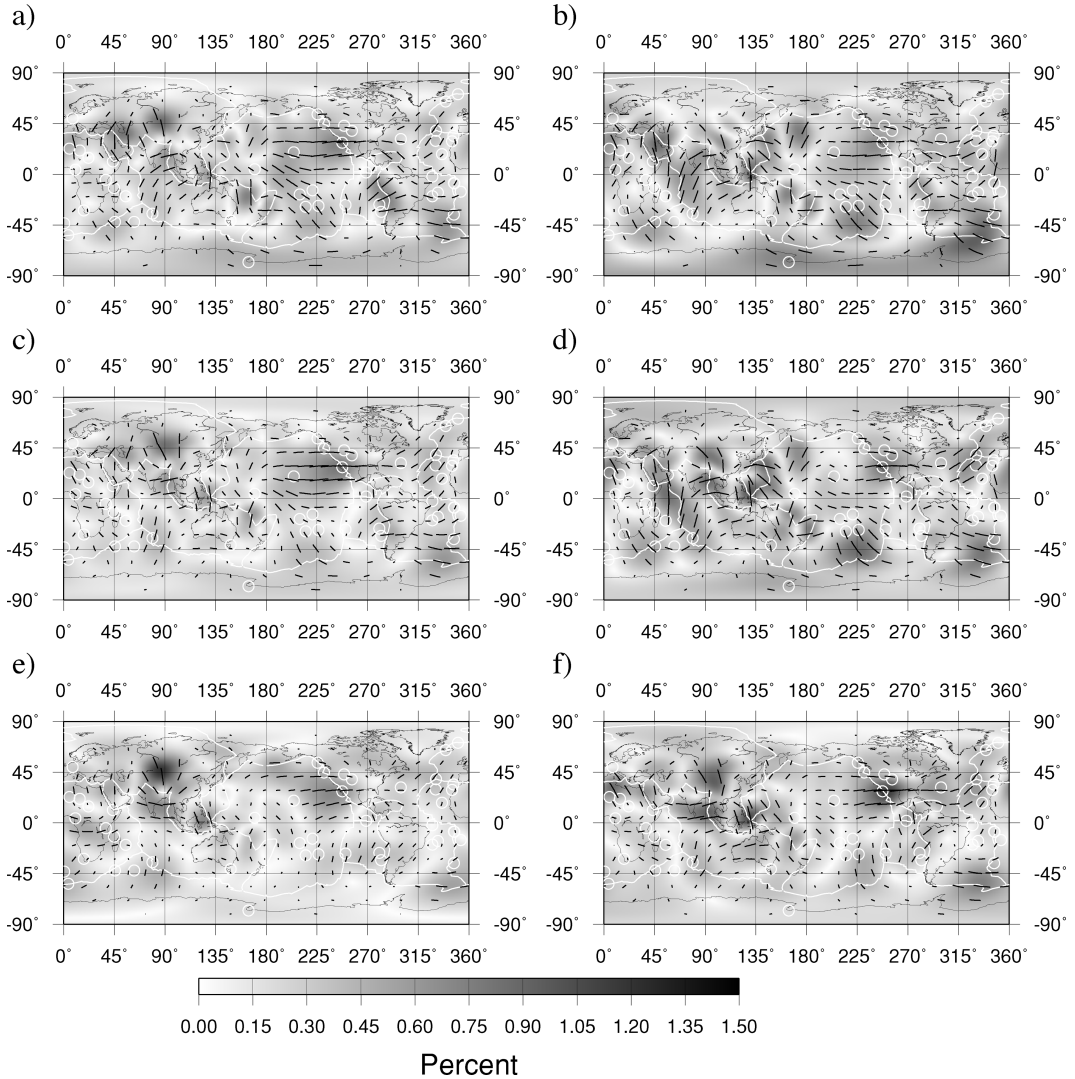

Figure 8. Azimuthally anisotropic 2ψ phase velocity maps for Rayleigh. The grey scale in the background corresponds to the peak-to-peak amplitude of anisotropy expressed relative to the average phase velocity calculated from PREM. The black lines represent the fast directions which are also scaled to the amplitude shown in the background. The plate boundaries and hotspots are indicated in white. Panels (a)–(f) show the different modes and periods as indicated in Fig. 6.

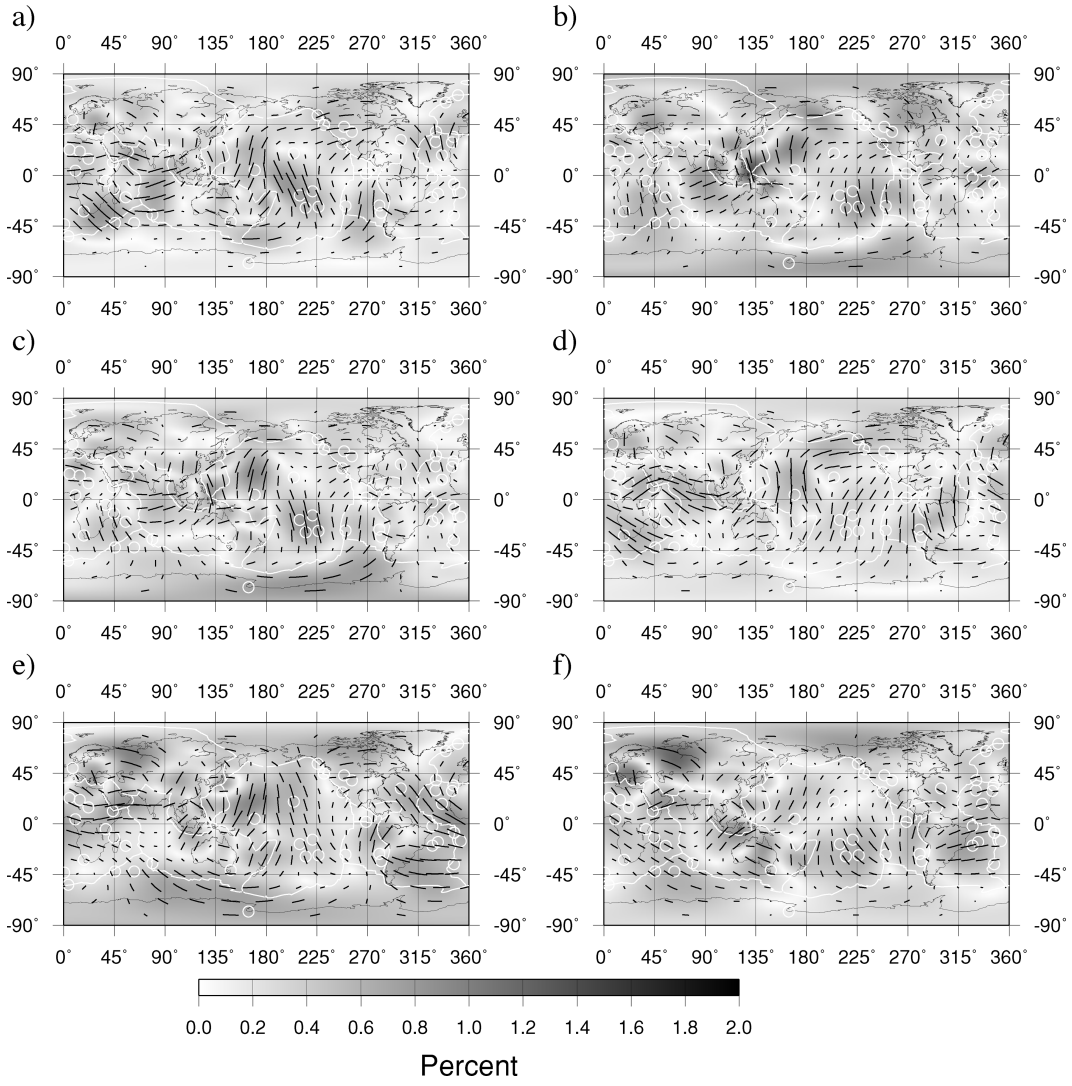

Figure 9. Azimuthally anisotropic 2ψ phase velocity maps for Love higher modes. Panels (a)–(f) show the different modes and periods as indicated in Fig. 7.

and sixth overtone are very sensitive to crustal structures. In general there is a good visual comparison between our maps and those of Van Heijst (1997). Visser *et al.* (2007) showed that higher modes can easily be measured with our technique. They showed isotropic degree 20 maps for illustration purposes. The correlation with our maps here up to degree 20 is around 0.80 for all Love wave overtones. The differences can be attributed to the neglect of anisotropy in the earlier paper.

The anisotropic contributions for the same higher modes and periods are shown in Figs 8 and 9 for the 2ψ term and Figs 10 and 11 for the 4ψ term. Fig. 12 shows the rms amplitude averaged over the sphere of the 2ψ and 4ψ maps for Rayleigh and Love waves for the fundamental up to the sixth higher mode with corresponding uncertainties. The amplitudes of the 2ψ and 4ψ term are similar within their standard deviations. Most importantly, the amplitude remains positive within the uncertainties, indicating that the anisotropic models are robust and indeed required, for the chosen optimal scaling. The 2ψ amplitudes even remain robust within two standard deviations. Figs 13 and 14 show some chosen 2ψ correlations and the corresponding ray theoretical sensitivity kernels (Larsen *et al.* 1998). For Rayleigh waves, the correlation of the fundamental mode models with the first higher mode ones is high (Fig. 13a). In fact, the correlation of the fundamental mode with increasingly higher modes consistently shows high values. The corresponding sensitivities show that the B–H sensitivity is mostly shallow for all modes while the G sensitivity changes with depth. This could indicate that B–H anisotropy is important for Rayleigh waves. We also find high correlations for modes where the most overlap is for deeper G, probably the transition zone anisotropy observed by Trampert & van Heijst (2002). For Love waves we obtain high correlations for G in the asthenosphere (Fig. 14). The correlation between the 2ψ models of the fundamental mode and first higher mode Love wave is quite low (<0.5), which is not surprising since G sensitivity for the fundamental mode is almost zero while it is non-zero for the first higher mode. The most likely source of 2ψ anisotropy in fundamental mode Love waves is B–H (Sieminski *et al.* 2007), while for the overtones G dominates, hence a plausible low correlation. These few examples illustrate how complex the depth distribution of azimuthal anisotropy possibly is, and only a depth inversion will provide detailed information about the specific distribution of the anisotropy. This will require finite frequency kernels (Sieminski *et al.* 2007) that capture the strong influence of path dependence and mode coupling for anisotropic parameters.

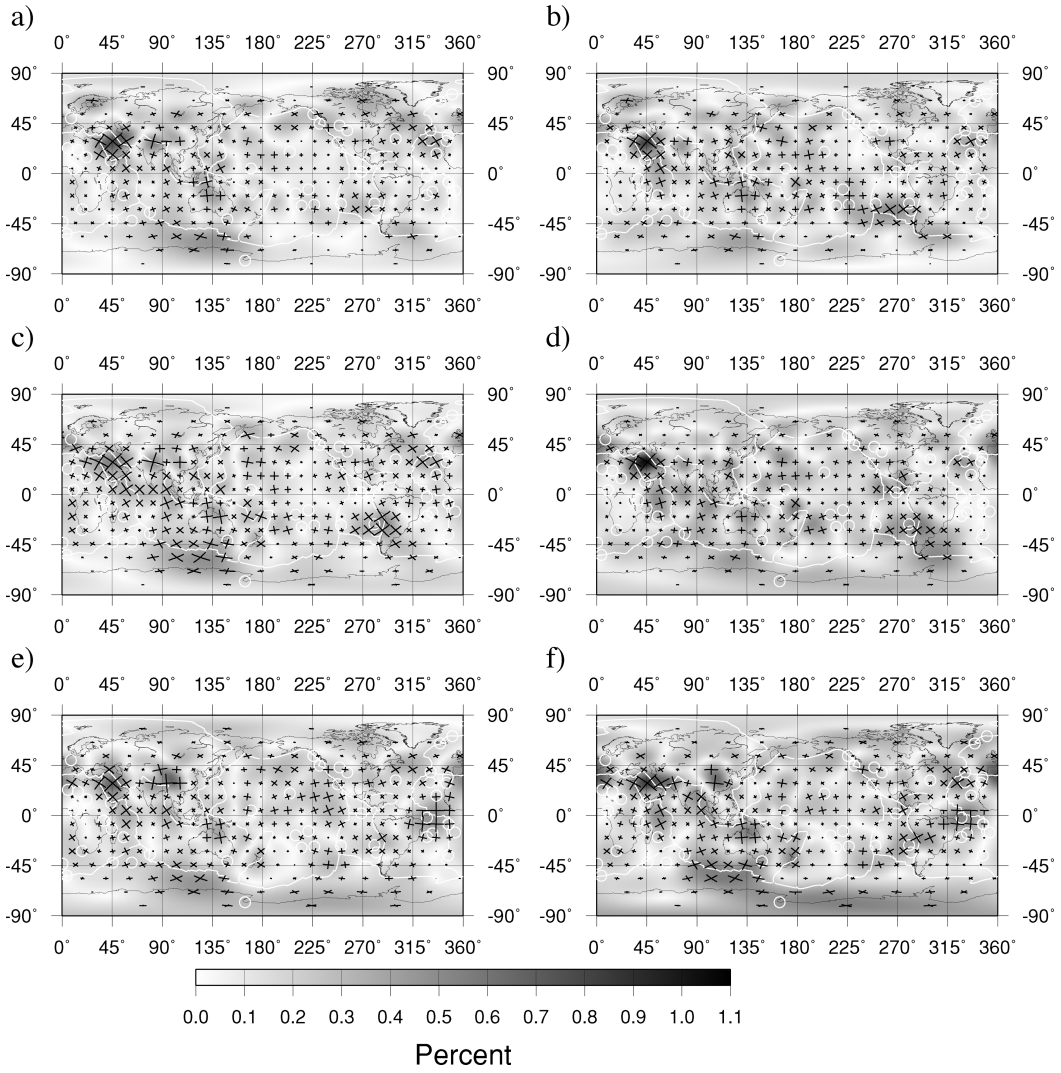

Figure 10. Azimuthally anisotropic 4ψ phase velocity maps for Rayleigh higher modes. Panels (a)–(f) show the different modes and periods as indicated in Fig. 6.

The fundamental mode 2ψ Rayleigh models visually agree at long wavelength with the models by Trampert & Woodhouse (2003), Ekström (2000) and in the Pacific with results obtained by Smith *et al.* (2004). Up to degree 8, we have a correlation of 0.49 with the 2ψ map of Trampert & Woodhouse (2003) for Rayleigh waves at 40 s. The first quantitative comparison between different azimuthally anisotropy models and geodynamic flow models was done by Becker *et al.* (2007). They found typical correlations between 0.18 and 0.47 indicating that our results are not at odds with any of these models. No comparison has been done for overtones. Only a detailed depth inversion can shed light on the geodymanic consequences of our 2ψ and 4ψ overtone maps.

Inverting for the azimuthal terms as well as the isotropic terms makes the isotropic maps become smoother for a given trace of the resolution. Decreasing overall damping will decrease the smoothness for both the isotropic, 2ψ and 4ψ phase velocity maps. We can split the total trace of the resolution matrix into the trace for the isotropic, 2ψ and 4ψ terms separately (Fig. 15). These individual values are more meaningful for the phase velocity maps than the total trace. The number of independent parameters for the isotropic, 2ψ and 4ψ terms varies as a function of overall damping. For small numbers of independently inverted parameters, the isotropic parameters dominate. As the number of independently inverted parameters increases, the number of inverted 2ψ and 4ψ parameters increases. Table 4 shows the total number of independently inverted parameters and the number of isotropic, 2ψ and 4ψ parameters for some chosen Rayleigh and Love wave fundamental and higher modes. For the fundamental mode models, we can resolve on average up to 25 spherical harmonic degrees for the isotropic models, 8 spherical harmonic degrees for the 2ψ models and 9 spherical harmonic degrees for the 4ψ models. For the higher modes, the number of degrees we can resolve decreases to degree 18 for the isotropic models, degree 5 for the 2ψ models and degree 6 for the 4ψ models.

Shapiro & Ritzwoller (2002) use a rms data misfit as a measure of uncertainty for the phase velocity maps. They obtain values around 25 m s^{-1} for fundamental mode Rayleigh and between 25 and 40 m s^{-1} for the fundamental mode Love wave phase velocity maps. The rms data misfit values we obtain for the fundamental mode are between 24 and 31 m s^{-1} for Rayleigh and 31–45 m s^{-1} for Love waves. The rms data misfit values for the higher modes are somewhat larger. They vary for Rayleigh waves between 35 and 65 m s^{-1} and for Love waves between 45 and 75 m s^{-1}. [Correction added after online publication 22 January 2008: units of km s^{-1} in the preceding sentence were corrected to m s^{-1}.]

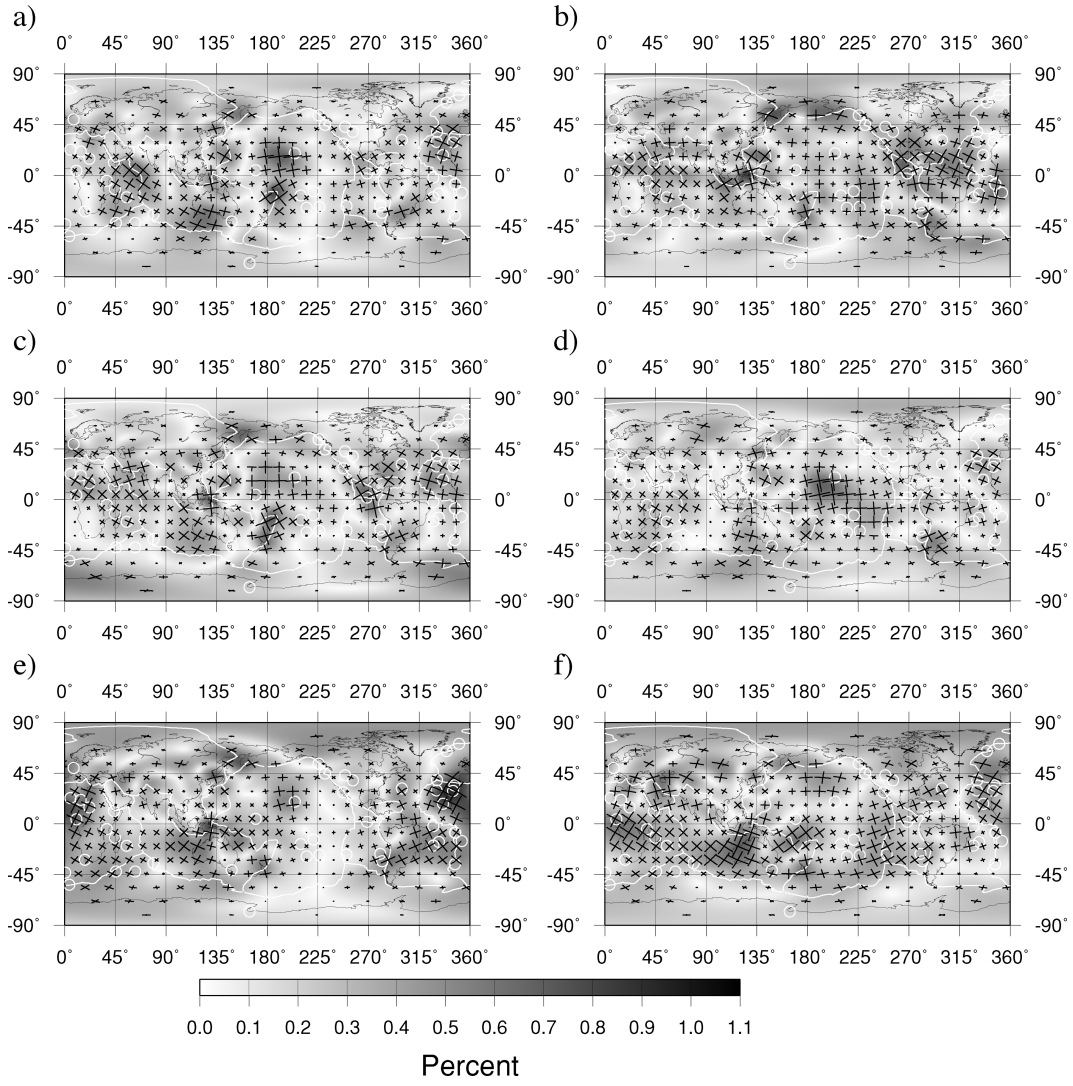

Figure 11. Azimuthally anisotropic 4ψ phase velocity maps for Love higher modes. Panels (a)–(f) show the different modes and periods as indicated in Fig. 7.

We are not so much interested in the posterior data uncertainties as in the posterior model uncertainties, which we need for a future depth inversion. The posterior model uncertainty is given by the posterior model covariance, defined as

$$\mathbf{C}_{\tilde{m}} = (\mathbf{I} - \mathbf{R})\mathbf{C}_m(\mathbf{I} - \mathbf{R})^T + \mathbf{L}\mathbf{C}_d\mathbf{L}^T, \tag{8}$$

where $\mathbf{C}_{\tilde{m}}$ is the posterior model covariance, $\mathbf{C}_m$ is the prior model covariance (eqs 4–6), $\mathbf{C}_d$ is the data covariance, $\mathbf{R}$ is the resolution matrix and $\mathbf{L}$ is the inverse operator which gives the estimated model $\tilde{\mathbf{m}} = \mathbf{L}\mathbf{d}$. The square roots of the diagonal elements of the posterior model covariance can be interpreted as error bars of the posterior values of the model parameters. An average posterior model uncertainty for a phase velocity map is obtained by taking the square root of the total power of the diagonal of the 0ψ, 2ψ and 4ψ terms averaged over the sphere. As explained above, we have chosen the overall damping (λ in $\mathbf{C}_m$) so that the average model uncertainty for $\widetilde{\mathrm{d}c/c_0}$ is constant. The value has been chosen so as to invert for 1000 independent parameters for 100 s fundamental mode Rayleigh waves. This gives average relative model uncertainties $\sigma_{\widetilde{\mathrm{d}c/c_0}}$ of 0.45, 0.18 and 0.15 per cent for the 0ψ, 2ψ and 4ψ maps (Fig. 16), respectively. The relative model uncertainty is much lower for the 2ψ and 4ψ maps due to the prior choice of a modest amount of anisotropy ($\theta_2 = \theta_4 = 0.1$). It is important to realise that a large part of $\mathbf{C}_{\tilde{m}}$ comes from the prior information, therefore, fixing $\mathbf{C}_{\tilde{m}}$ will require different λ in $\mathbf{C}_m$ depending on $\mathbf{C}_d$ and the number of data and this will change $\mathbf{R}$ correspondingly.

The absolute uncertainties ($\sigma_{\widetilde{\mathrm{d}c}}$, Fig. 16) in the fundamental mode Rayleigh isotropic models range from 15 m s^{-1} at short periods to 20 m s^{-1} at longer periods, the uncertainty of the 2ψ models range from 5 to 8 m s^{-1} and the uncertainty of the 4ψ models range from 5 to 7 m s^{-1}. For Love waves, the corresponding absolute uncertainties for the fundamental mode isotropic maps ranges from 14 to 20 m s^{-1}, for the 2ψ models from 5 to 8 m s^{-1} and the 4ψ models from 4 to 7 m s^{-1}. The rms data misfit values given earlier show uncertainties for both Love and Rayleigh wave azimuthal anisotropic models in the order of 25–45 m s^{-1} for the fundamental mode. The absolute model uncertainties are a bit smaller but of the same order of magnitude as the rms data misfits, justifying the intuition of Shapiro & Ritzwoller (2002) to use the data misfits as average model uncertainties. The reason for this good correspondence is that the data misfit incorporates the prior information in eq. (8) implicitly.

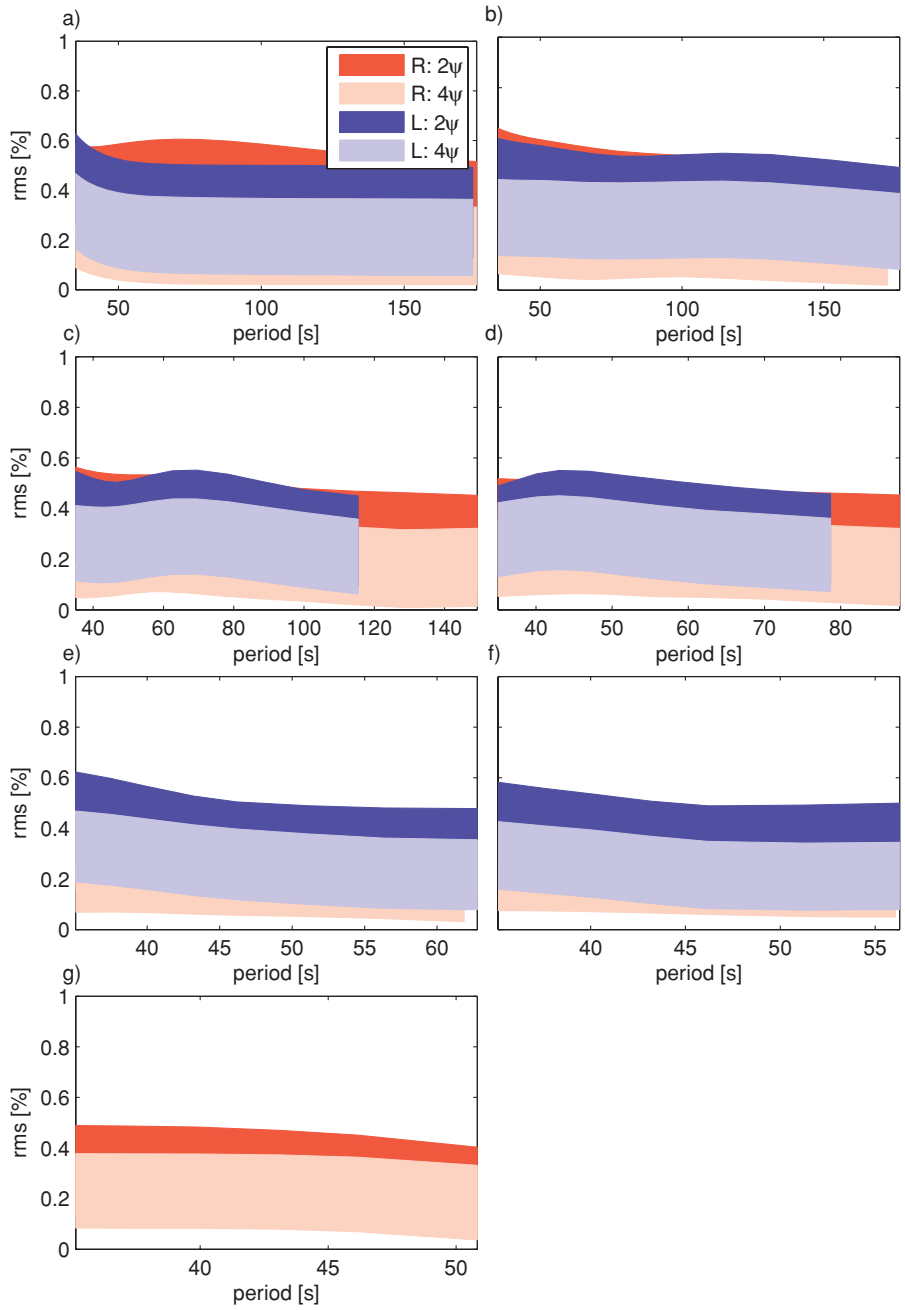

Figure 12. The rms amplitude per unit sphere of the phase velocity maps of Figs 8 to 11 for (a) the fundamental mode, (b) the first higher mode, (c) the second higher mode, (d) the third higher mode, (e) the fourth higher mode, (f) the fifth higher mode and (g) the sixth higher mode. The bands correspond to ± one standard deviation of the fixed average posterior uncertainty.

6 RESOLUTION AND TRADE-OFF

The fifth higher mode Love wave data set has the lowest number of measurements. The number of measurements increases with lower overtone number (Table 2). Nevertheless the pattern of ray density for the fifth higher mode Love wave is quite similar to the fundamental mode Rayleigh wave which contains the highest number of measurements. Trampert & Woodhouse (1995) converted the resolution matrix into averaging kernels. The relative phase velocity perturbation at a specific point on the Earth is an average of the true model over the whole Earth with weights (the averaging kernels). For a complete picture of resolution the averaging kernels have to be calculated at each point on the Earth's surface. Trampert & Woodhouse (1995) chose to represent the averaging kernels by the radius of the central peak and called the maps resolving radii maps. The resolving radii are only dependent upon path coverage and the overall damping (λ) and give a good representation of the lateral resolution that can be achieved. The number of measurements of the fifth higher mode Love wave correspond to the number of measurements of the fundamental Love waves in Trampert & Woodhouse (1995) and the corresponding resolving radii map (fig. 7a in Trampert & Woodhouse 1995) corresponds to the resolving radii map of the fifth higher mode Love wave (our worst data coverage). There is a high correspondence with the ray density map but the resolving

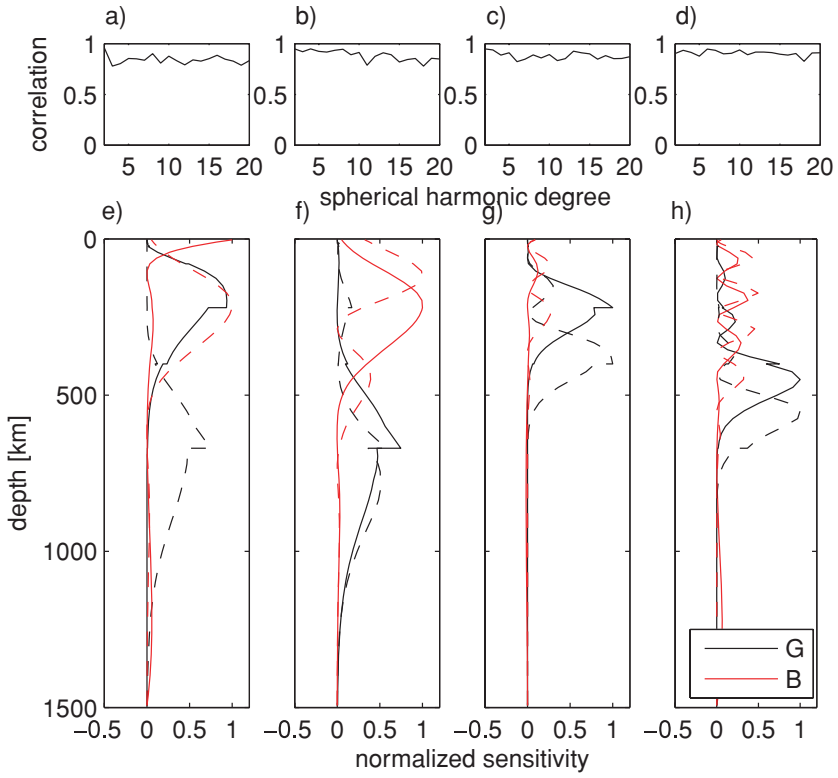

Figure 13. Rayleigh 2ψ correlation (a–d) and 2ψ sensitivity kernels (e–h) of the fundamental mode at 151 s (solid) with the first higher mode at 149 s (dashed) (a, e), the first higher mode at 149 s (solid) with the second higher mode at 99 s (dashed) (b, f), the first higher mode at 40 s (solid) with the second higher mode at 40 s (dashed) (c, g) and the third higher mode at 35 s (solid) with the fourth higher mode at 35 s (dashed) (d, h). Sensitivity to H is not shown since it is similar to B sensitivity but opposite in sign.

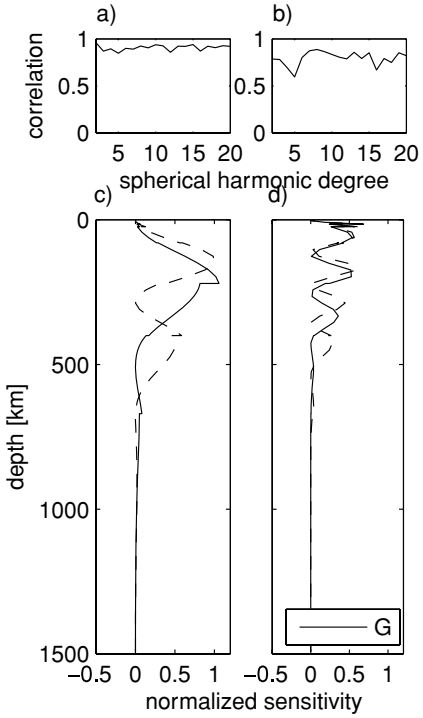

Figure 14. Love 2ψ correlation (a, b) and 2ψ sensitivity kernels (c, d) of the first higher mode at 153 s (solid) with the second higher mode at 100 s (dashed) (a, c) and the third higher mode at 35 s (solid) with the fourth higher mode at 35 s (dashed) (b, d).

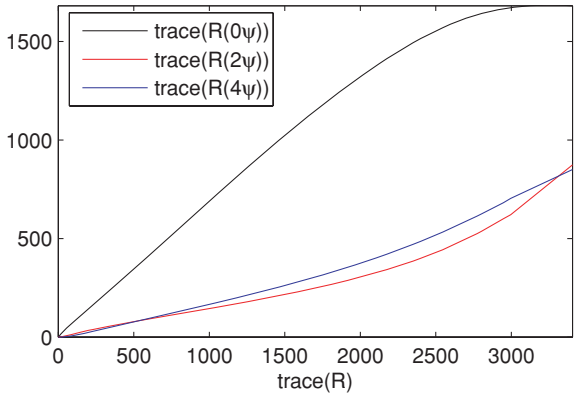

Figure 15. The relation between the total trace of the resolution matrix and the trace of the resolution matrix separated for the isotropic, 2ψ and 4ψ terms for the fundamental mode Rayleigh wave at 151 s.

radii test gives a better indication of the structures we are able to solve for.

There are three different issues that affect the resolution; spectral leakage, trade-off between the isotropic and anisotropic terms and damping. Spectral leakage is caused by the mapping of small-scale structure not accounted for in the model expansion into the inverted low-degree structure and is a result of uneven data coverage (Snieder *et al.* 1991). Spectral leakage can be suppressed by a time consuming operator (Trampert & Snieder 1996) or approximately by Laplacian damping (Spetzler & Trampert 2003) as in eqs (4)–(6) $\{\frac{1}{[l(l+1)]^2}\}$. The price to pay for this Laplacian damping is that the higher the

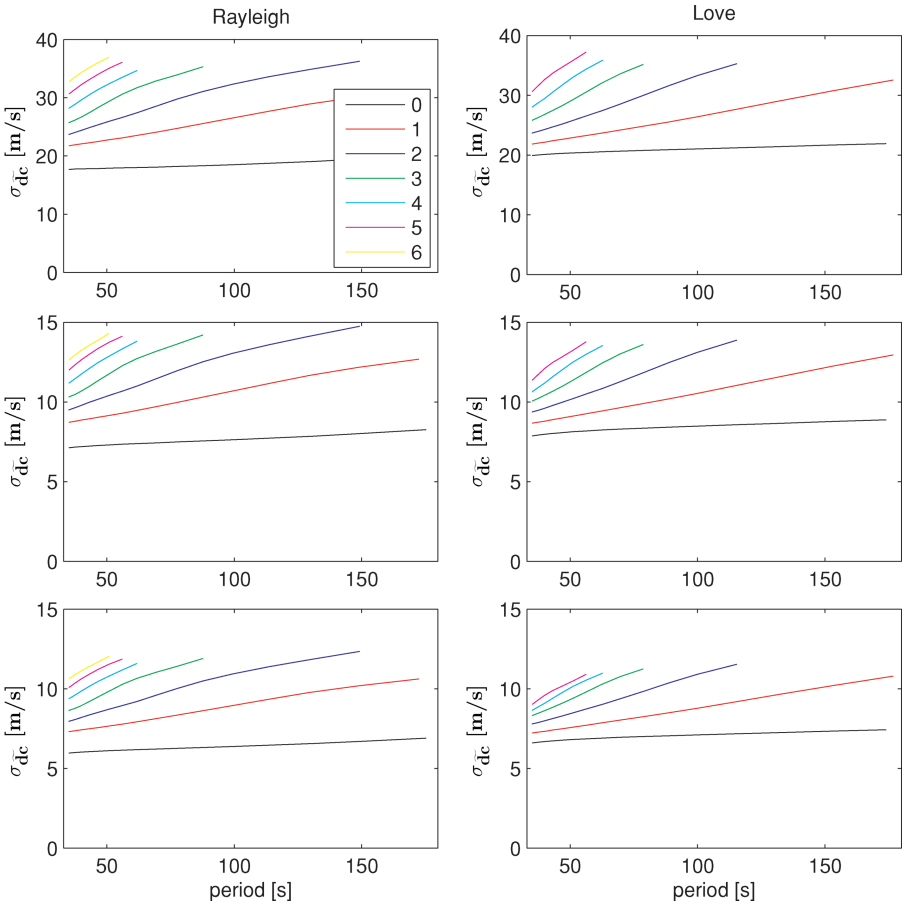

Figure 16. Absolute standard deviations for the fundamental and first six higher mode Rayleigh wave isotropic (top left-hand panel), 2ψ (middle left-hand panel) and 4ψ (bottom left-hand panel) phase velocity maps. The same for the fundamental and first five higher mode Love waves on the right-hand side.

degree, the less it will be resolved and the diagonal peak of the resolution matrix will also broaden. Finally there will be trade-offs between the isotropic and anisotropic parameters. The resolution matrix provides information on the trade-offs and the broadening (Fig. 17). The diagonal of the resolution matrix shows the price we pay for the use of Laplacian damping. For higher degrees, the diagonal values of the resolution matrix decrease. The choice of the relative strength of anisotropy (θ_2, $\theta_4 = 0.1, 0.1$) causes the sharper decay for the 2ψ and 4ψ parameters. Table 4 shows the number of resolved parameters for certain modes given our choice of overall damping described above. The off-diagonal terms of the resolution matrix in Fig. 17 show the amount of broadening and trade-off between parameters. Fortunately, these values are small compared to the diagonal values. This holds for all higher modes.

7 CONCLUSIONS

We present global azimuthal anisotropic phase velocity maps for the fundamental modes and up to the sixth overtone for Rayleigh waves and up to the fifth overtone for Love waves. Phase velocities for fundamental and higher mode Love and Rayleigh waves were measured using a model space search approach (Visser *et al.* 2007). The use of a model space search approach enables us to obtain realistic and consistent uncertainties on the phase velocities. The phase velocities are inverted to extract azimuthal anisotropic phase velocity maps. Following Trampert & Woodhouse (2003), we determine the optimum relative weighting prior to inversion. Both Love and Rayleigh fundamental and higher mode phase velocities require anisotropy according to the misfit curves. The relative weighting was chosen (in agreement with the significant difference of misfit curves) such that anisotropy is needed and equal for the 2ψ and the 4ψ terms of anisotropy. We have chosen the overall damping such that the relative uncertainty is constant in all maps. This causes the resolution to decrease with increasing data uncertainty and/or decreasing number of data.

The rms data misfits of the azimuthal anisotropic models for fundamental mode Rayleigh and Love waves are similar to values found by Shapiro & Ritzwoller (2002). The rms misfits for the higher modes are larger and vary between 35 and 65 m s^{-1} for Rayleigh and between 45 and 75 m s^{-1} for Love waves. [Correction added after online publication 22 January 2008: a unit of km s^{-1} in the preceding sentence was corrected to m s^{-1}.] The model uncertainties are smaller than the rms data misfits but of the same order. For the fundamental mode isotropic models, we obtain uncertainties up to 20 m s^{-1} and for the anisotropic models we obtain uncertainties up to 8 m s^{-1}.

The isotropic maps visually compare well with the isotropic higher mode maps of Van Heijst (1997). We found a high correlation with the fundamental mode anisotropic maps of Trampert & Woodhouse (2003) and hence with equivalent work from other research groups (Becker *et al.* 2007). Indications are that the source of azimuthal anisotropy is complex and a detailed depth inversion, using finite frequency kernels, is needed to clarify this. Our efforts to provide maps for many overtones, should facilitate this final step in the search of deep anisotropy.

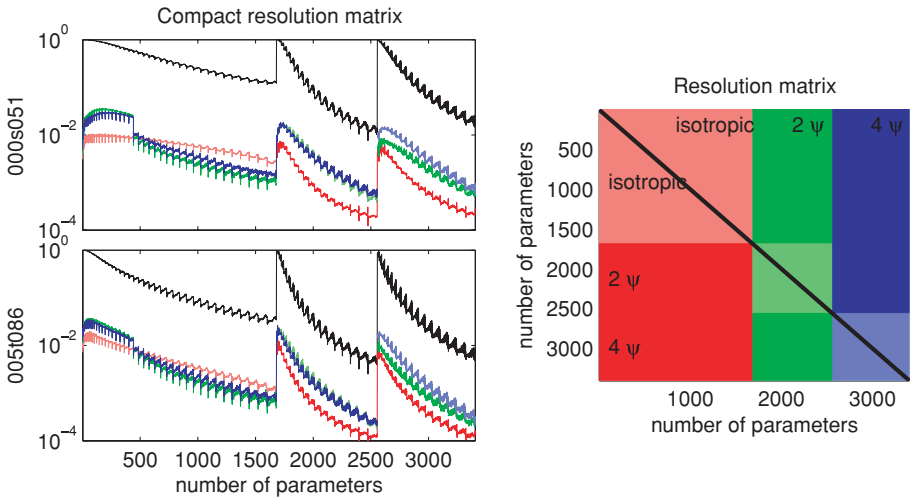

Figure 17. The resolution matrix for the fundamental mode Rayleigh (top left-hand figure) and the fifth higher mode Love (bottom left-hand figure). The figure on the right-hand side shows how the left-hand side figures are related to the resolution matrix. Each row of the matrix is shown in the figures, where black is the trace of the resolution matrix, red is the rms of the isotropic parameters (not including the diagonal) for that row, green represents the rms of the 2ψ parameters for the specific row and blue the rms of the 4ψ parameters for the specific row. The off-diagonal terms within one parameter family are given by the lighter shaded colours, red for the isotropic parameters, green for the 2ψ parameters and blue for the 4ψ parameters. The darker shaded lines represent the trade-off between isotropic/2ψ/4ψ terms.

ACKNOWLEDGMENTS

We would like to thank two anonymous reviewers for their constructive comments and Anne Sieminski for fruitful discussion. The higher mode phase velocity measurements were measured using seismograms that were provided by the GDSN and GEOSCOPE networks and obtained via the IRIS database. The computational resources for this work were provided by the Netherlands Research Center for Integrated Solid Earth Sciences (ISES 3.2.5 High End Scientific Computation Resources). Figs 1, 2 and 6–12 were generated using the Generic Mapping Tools (GMT) (Wessel & Smith 1995).

REFERENCES

Aki, K. & Kaminuma, K., 1963. Love waves from the Aleutian shock of March 9, 1957, *Bull. Earthq. Res. Instit.,* **41,** 243–259.

Anderson, D.L., 1961. Elastic wave propagation in layered anisotropic media, *J. geophys. Res.,* **66,** 2953–2963.

Becker, T.W., Ekström, G., Boschi, L. & Woodhouse, J.H., 2007. Length scales, patterns, and origin of azimuthal seismic anisotropy in the upper mantle as mapped by Rayleigh waves, *Geophys. J. Int.,* **171,** 451–462.

Beucler, E. & Montagner, J., 2006. Computation of large anisotropic seismic heterogeneities (CLASH), *Geophys. J. Int.,* **165,** 447–468.

Bevington, P.R. & Robinson, D.K., 1992. *Data Reduction and Error Analysis for the Physical Sciences,* McGraw-Hill, New York.

Debayle, E. & Kennett, B.L.N., 2000. Anisotropy in the Australian upper mantle from Love and Rayleigh waveform inversion, *Earth planet. Sci. Lett.,* **184,** 339–351.

Deschamps, F., Snieder, R. & Trampert, J., 2001. The relative density to shear velocity scaling in the uppermost mantle, *Phys. Earth planet. Inter.,* **124,** 193–211.

Dziewonski, A.M. & Anderson, D.L., 1981. Preliminary reference earth model, *Phys. Earth Planet. Inter.,* **25,** 297–356.

Ekström, G., 2000. Mapping the lithosphere and asthenosphere with surface waves: lateral structure and anisotropy, *The History and Dynamics of Global Plate Motions, Geophys. Monogr. Ser.,* **121,** 211–238.

Ekström, G. & Dziewonski, A.M., 1998. The unique anisotropy of the Pacific upper mantle, *Nature,* **394,** 168–172.

Forsyth, D.W., 1975. The early structural evolution and anisotropy of the oceanic upper mantle, *Geophys. J. R. astr. Soc.,* **43,** 103–162.

Hess, H.H., 1964. Seismic anisotropy of the uppermost mantle under oceans, *Nature,* **203,** 629–631.

Karato, S., 1998. Seismic anisotropy in the deep mantle, boundary layers and the geometry of mantle convection, *Pure appl. Geophys.,* **151,** 565–587.

Larsen, E.W.F., Tromp, J. & Ekström, G., 1998. Effects of slight anisotropy on surface waves, *Geophys. J. Int.,* **132,** 654–666.

Lebedev, S., Nolet, G., Meier, T. & van der Hilst, R.D., 2005. Automated multimode inversion of surface and S waveforms, *Geophys. J. Int.,* **162,** 951–964.

Maggi, A., Debayle, E., Priestley, K. & Barruol, G., 2006. Multimode surface waveform tomography of the Pacific Ocean: a closer look at the lithospheric cooling signature, *Geophys. J. Int.,* **166,** 1384–1397.

McEvilly, T.V., 1964. Central US crust-upper mantle structure from Love and Rayleigh wave phase velocity inversion, *Bull. seism. Soc. Am.,* **54,** 1997–2015.

Montagner, J.P., 1998. Where can seismic anisotropy be detected in the Earth's mantle? *Pure appl. Geophys.,* **151,** 223–256.

Montagner, J.P. & Nataf, H.C., 1986. A simple method for inverting the azimuthal anisotropy of surface waves, *J. geophys. Res.,* **91,** 511–520.

Montagner, J. & Tanimoto, T., 1990. Global anisotropy in the upper mantle inferred from the regionalization of phase velocities, *J. geophys. Res.,* **95,** 4794–4819.

Montagner, J.P. & Tanimoto, T., 1991. Global upper mantle tomography of seismic velocities and anisotropies, *J. geophys. res.,* **96,** 20 337–20 351.

Nataf, H.C., Nakanishi, I. & Anderson, D.L., 1984. Anisotropy and shear velocity heterogeneity in the upper mantle, *Geophys. Res. Lett.,* **11,** 109–112.

Ritsema, J. & Van Heijst, H., 2002. Constraints on the correlation of P- and S-wave velocity heterogeneity in the mantle from P, PP, PPP and PKPab traveltimes, *Geophys. J. Int.,* **149,** 482–489.

Romanowicz, B. & Snieder, R., 1988. A new formalism for the effect of lateral heterogeneity on normal modes and surface waves, II: general anisotropic perturbations, *Geophys. J. R. astr. Soc.,* **93,** 91–99.

Sambridge, M., 1999a. Geophysical inversion with a neighbourhood algorithm-I. Searching a parameter space, *Geophys. J. Int.,* **138,** 479–494.

Sambridge, M., 1999b. Geophysical inversion with a neighbourhood algorithm-II. Appraising the ensemble, *Geophys. J. Int.,* **138,** 727–746.

Sebai, A., Stutzmann, E., Montagner, J.P., Sicilia, D. & Beucler, E., 2006. Anisotropic structure of the African upper mantle from Rayleigh and Love wave tomography, *Phys. Earth planet. Inter.,* **155,** 48–62.

Shapiro, N.M. & Ritzwoller, M.H., 2002. Monte-Carlo inversion for a global shear-velocity model of the crust and upper mantle, *Geophys. J. Int.,* **151,** 88–105.

Sieminski, A., Liu, Q., Trampert, J. & Tromp, J., 2007. Finite-frequency sensitivity of surface waves to anisotropy based upon adjoint methods, *Geophys. J. Int.,* **168,** doi:10.1111/j.1365–246X.2006.03261.x.

Simons, F., van der Hilst, R., Montagner, J. & Zielhuis, A., 2002. Multimode Rayleigh wave inversion for heterogeneity and azimuthal anisotropy of the Australian upper mantle, *Geophys. J. Int.,* **151,** 738–754.

Smith, D.B., Ritzwoller, M.H. & Shapiro, N.M., 2004. Stratification of anisotropy in the Pacific upper mantle, *J. geophys. Res.,* **109,** B11309, doi:10.1029/2004JB003200.

Smith, M.L. & Dahlen, F.A., 1973. The azimuthal dependence of Love and Rayleigh wave propagation in a slightly anisotropic medium, *J. geophys. Res.,* **78,** 3321–3333.

Smith, M.L. & Dahlen, F.A., 1975. Correction to: 'The azimuthal dependence of Love and Rayleigh wave propagation in a slightly anisotropic medium', *J. geophys. Res.,* **80,** 1923.

Snieder, R., Beckers, J. & Neele, F., 1991. The effect of small-scale structure on normal mode frequencies and global inversions, *J. geophys. Res.,* **59,** 501–515.

Spetzler, J. & Trampert, J., 2003. Implementing spectral leakage corrections in global surface wave tomography, *Geophys. J. Int.,* **155,** 532–538.

Tanimoto, T. & Anderson, D.L., 1984. Mapping convection in the mantle, *Geophys. Res. Lett.,* **11,** 287–290.

Trampert, J. & Snieder, R., 1996. Model estimates biased by truncated expansions: possible artifacts in seismic tomography, *Science,* **271,** 1257–1260.

Trampert, J. & van Heijst, H.J., 2002. Global azimuthal anisotropy in the transition zone, *Science,* **296,** 1297–1299.

Trampert, J. & Woodhouse, J.H., 1995. Global phase velocity maps of Love and Rayleigh waves between 40 and 150 seconds, *Geophys. J. Int.,* **122,** 675–690.

Trampert, J. & Woodhouse, J.H., 2003. Global anisotropic phase velocity maps for fundamental mode surface waves between 40 and 150 s, *Geophys. J. Int.,* **154,** 154–165.

Van Heijst, H.J., 1997. New constraints on the seismic structure of the Earth from surface wave overtone phase velocity measurements, *D. Phil. thesis*, University of Oxford.

Vinnik, L.P., Farra, V. & Romanowicz, B., 1989. Azimuthal anisotropy in the Earth from observations of SKS at GEOSCOPE and NARS broad-band stations, *Geophys. J. Int.,* **79,** 1542–1558.

Visser, K., Lebedev, S., Trampert, J. & Kennett, B.L.N., 2007. Global love wave overtone measurements, *Geophys. Res. Lett.,* **34,** L03302, doi:10.1029/2006GL028671.

Wessel, P. & Smith, W.H.F., 1995. New version of the generic mapping tools released, *EOS, Trans. Am. geophys. Un.,* **76,** 329.

Yoshizawa, K. & Kennett, B.L.N., 2002. Non-linear waveform inversion for surface waves with a neighbourhood algorithm - application to mulitmode dispersion measurements, *Geophys. J. Int.,* **149,** 118–133.